# Steered Molecular Dynamics Studies of the Potential of Mean Force of a $Na^+$ or $K^+$ Ion in a Cyclic Peptide Nanotube

**Hyonseok Hwang, George C. Schatz,* and Mark A. Ratner***

*Department of Chemistry, Northwestern University, 2145 Sheridan Road, Evanston, Illinois 60208-3113*

*Received: September 5, 2006; In Final Form: October 17, 2006*

Potential of mean force (PMF) profiles of a single $Na^+$ or $K^+$ ion passing through a cyclic peptide nanotube, cyclo[-(D-Ala-Glu-D-Ala-Gln)$_2$-], in water are calculated to provide insight into ion transport and to understand the conductance difference between these two ions. The PMF profiles are obtained by performing steered molecular dynamics (SMD) simulations that are based on the Jarzynski equality. The computed PMF profiles for both ions show barriers of around 2.4 kcal/mol at the channel entrances and exits and energy wells in the middle of the tube. The energy barriers, so-called dielectric energy barriers, arise due to the desolvation of water molecules when ions move across the nanotube, and the energy wells appear as a result of attractive interactions between the cations and negatively charged carbonyl oxygens on the backbone of the tube. We find more and deeper energy wells in the PMF profile for $Na^+$ than for $K^+$, which suggests that $Na^+$ ions have a longer residence time inside the nanotube and that permeation of $Na^+$ ions is reduced compared to $K^+$ ions. Calculations of the radial distribution functions (RDF) between the ions and oxygens in the water molecules and in carbonyl groups on the tube and an investigation of the orientations of the carbonyl groups show that, in contrast with the dynamic carbonyl groups observed in the selectivity filter of the KcsA ion channel, the carbonyl groups in the cyclic peptide nanotube are relatively rigid, with only slight reorientation of the carbonyl groups as the cations pass through. The rigidity of the carbonyl groups in the cyclic peptide nanotube can be attributed to their role in hydrogen bonding, which is responsible for the tube structure. Comparison of the PMF profiles with the electrostatic energy profiles calculated from the Poisson−Boltzmann (PB) equation, a dielectric continuum model, reveals that the dielectric continuum model breaks down in the confined region within the tube that governs ion transport.

## I. Introduction

Ion channels are proteins, found in cell membranes, that transport ions across the membranes.[1−3] Ion channels play a crucial role in biological processes such as nerve and muscle excitation, hormone secretion, and sensory transduction.[4] Malfunctioning ion channels often cause profound physiological effects. Due to their important functional roles, many studies have been devoted to better understanding ion channels.

Cyclic peptide nanotubes are a class of artificial ion channels that are formed from closed peptide rings, each having an even number of alternating D- and L-amino acid residues.[5−9] Hydrogen bonding among the peptide rings drives them into a self-assembled tubular structure. Depending on the hydrophilic or hydrophobic nature of side chains, the cyclic peptide nanotubes can be found either in water solution or in lipid bilayer membranes.[5,6,9] When embedded in membranes, they have potentially useful properties related to ion transport, including ion rectification[10] and antibacterial activity.[11]

From a theoretical viewpoint, the cyclic peptide nanotubes provide new insight into many classes of natural and artificial ion channels because they share structural and functional similarities with other channels, including the use of carbonyl groups to form the backbone of the tube and the presence of water inside the tube. Several theoretical and computational works have been done to better understand the structure and dynamics of the cyclic peptide nanotubes. The dynamics of water inside a cyclic peptide nanotube with hydrophilic side chains was investigated with molecular dynamics (MD) simulations by Engles et al.[12] They determined the equilibrium arrangement of water molecules inside the tube and computed a water diffusion coefficient that is lower than that for bulk water. Asthagiri and Bashford calculated the solvation free energies of several ions inside a simple model cyclic peptide nanotube with various methods and compared the results from each method.[13] Khurana et al. studied the self-assembly of cyclic peptide dimers in polar and nonpolar solvents with MD simulations.[14] Hwang et al. applied Poisson−Nernst−Planck (PNP) theory[15,16] to obtain ion current−voltage curves for cyclic peptide nanotubes embedded in different types of membrane bilayers.[17]

The potential of mean force (PMF) is the free energy as a function of a reaction coordinate or as a function of a chosen order parameter.[18] This is a useful property to examine in studies of ion permeation inside cyclic peptide nanotubes or ion channels, as it provides mechanistic insight about the transport mechanism, so there have been many studies of the PMF for natural ion channels. For example, Allen and co-workers used umbrella sampling to perform PMF calculations for transport of $K^+$ across the gramicidin A channel, and they determined the effect of the ion channel structure, the membrane, and water on the PMF profile.[19,20] Also, Liu et al. determined the PMF profile for transport of a single $Na^+$ ion through the gramicidin A channel, including explicit water and the membrane bilayer

* Corresponding authors. E-mail: g-schatz@northwestern.edu (G.C.S.) and ratner@chem.northwestern.edu (M.A.R.).

10.1021/jp0657888 CCC: $33.50 
Published on Web 12/05/2006

in calculations that were performed using steered molecular dynamics (SMD) simulations to elucidate the ion conductance mechanism.[21]

PMF profiles depend on the entropy of the system as well as intra- and intermolecular interactions, so the calculation of the PMF in condensed phases has long been a challenge to computer simulations. One of the several methods that have been developed for PMF calculations is umbrella sampling, which uses a biasing potential to obtain better sampling in thermodynamically unfavorable regions.[22−24] Recently, the construction of PMF profiles from SMD simulations has been proposed.[25−28] SMD simulations, where a molecule or an ion of interest is steered by an imaginary atomic force microscopy (AFM) tip, are based on the Jarzynski equality theorem,[29,30] which enables us to obtain a PMF profile from a nonequilibrium MD calculation. Although optimized parameters such as the pulling velocity and the harmonic constraint connecting the imaginary tip to the molecule of interest need to be determined before the SMD simulation, this approach supplies an effective way to explore the PMF of a condensed phase system.

In this work, we use SMD simulations to calculate the PMF profiles for $Na^+$ or $K^+$ inside a cyclic peptide nanotube that is composed of four cyclo[-(D-Ala-Glu-D-Ala-Gln)$_2$-] subunits (Figure 1) in water.[5] In Figure 1, the α-plane regions are defined as the regions near the plane of the peptide $C_\alpha$ atoms in a cyclic peptide ring and midplane regions are the regions between two α-plane zones.[12] The nanotube is assumed dissolved in water due to its hydrophilic side chains. The measured difference between the ion conductivity of $Na^+$ and $K^+$ ions[5] is then interpreted on the basis of the calculated difference in PMF profiles for the two ions. The effects of the electrostatic interactions between the ions and water and between the ions and fixed charges in the cyclic peptide nanotube on the PMF profiles are also investigated. The Poisson−Boltzmann (PB) equation, which is based on a dielectric continuum model, is also employed to show the breakdown of that model in the confined region inside the ion channel. Although the cyclic peptide nanotube in this study is surrounded by water molecules, which is in contrast with usual cyclic peptide nanotubes that are embedded in lipid bilayer membranes, we believe that the current study will provide useful insight for understanding ion permeation in more complex systems.

This Article is organized as follows. In the next section, our system is introduced and simulation methods including the SMD simulation are briefly reviewed. Results are presented in Section III, and a discussion and conclusions are provided in the final section. Limitations of the present work and further studies are also discussed in that section.

## II. Theory and Methods

**A. Description of the Simulations.** We consider a system composed of one peptide nanotube and one ion surrounded by water molecules, in accord with an earlier study by Ghadiri and co-workers.[5] The peptide nanotube is formed by four cyclo-[-(D-Ala-Glu-D-Ala-Gln)$_2$-] rings (See Figure 1). Due to the hydrophilic nature of the side chains, the nanotube dissolves in water. The protonated form of the glutamic acid is used because cyclic peptide rings with the protonated acid self-assemble more easily due to their lesser solubility.[5] The number of cyclic peptide rings is somewhat arbitrary, so we chose four rings to reduce the computational load. The results we present later suggest that this short nanotube can still capture the thermodynamic properties of any length of cyclic peptide nanotube.

The initial structure of the backbone of the nanotube was built from scratch on the basis of the information provided by the experiments and earlier simulations.[5,6,12] The side chains were prepared from the molecular modeling package SPARTAN 2004.[31] The energy minimization of the peptide nanotube was carried out with the CHARMM27 force field[32] using the NAMD simulation code, version 2.5.[33] In the energy-minimized structure of the nanotube, the average distance between two cyclic peptide rings is about 4.7 Å and the average radius of a ring from the central axis to $C_\alpha$ atoms on the tube is 4.87 Å. This energy-minimized structure was used as a reference for all the simulations in this work.

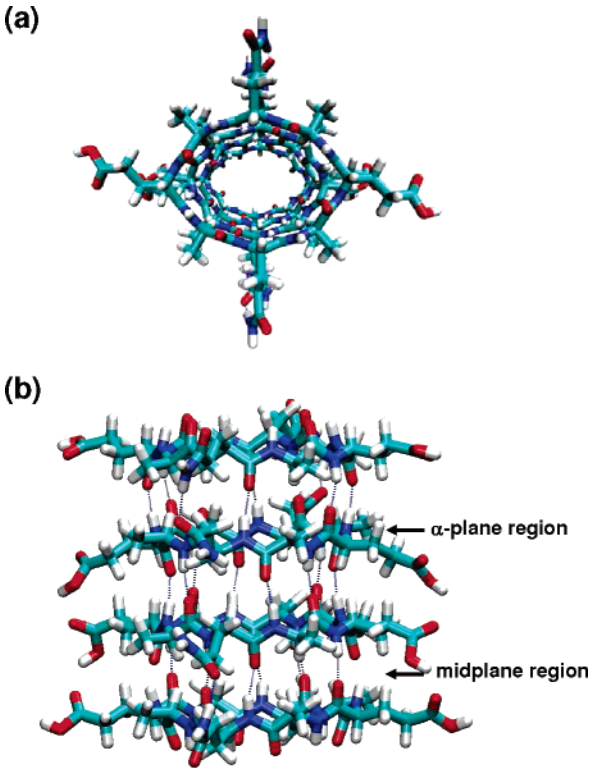


**Figure 1.** (a) Top view and (b) side view of a cyclic peptide nanotube, 4 × cyclo[(D-Ala-Glu-D-Ala-Gln)$_2$]. Hydrogen bonds between the cyclic peptide rings are represented with dotted lines. α-Plane and midplane regions are defined in the text following the work in ref 12.

The $Na^+$ or $K^+$ ion was inserted at a position along the *z*-axis of the nanotube, and water molecules were randomly positioned and oriented around the nanotube to avoid poor van der Waals interactions. The number of water molecules in the system was calculated based on a partial volume of 1.00 $cm^3/g$ for water and 0.73 $cm^3/g$ for the nanotube. The complete system is composed of one nanotube, one cation, and 1131 water molecules in a simulation box whose dimensions are 31.5 × 31.5 × 38.0 Å.

The system was investigated using the canonical (NVT) ensemble with periodic boundary conditions. A Langevin dynamics method was implemented to maintain the temperature of the system at 298 K. The equation of motion was integrated with a time step of 2 fs for the equilibrations and 1 fs for SMD simulations. The bonds between each hydrogen and its parent atom were constrained to their equilibrium values by the SHAKE algorithm. The CHARMM27 force field[32] and TIP3P water model[34] were used to describe the nanotube and water molecules, respectively. The force fields for the ion interactions were obtained from Beglov and Roux.[35] Long-range electrostatic interactions were treated using the particle mesh Ewald (PME) method with conducting (tinfoil) boundary conditions. A tolerance of $10^{-6}$ and a cutoff distance of 12 Å were applied to the direct space sum of the Coulomb interaction. The reciprocal

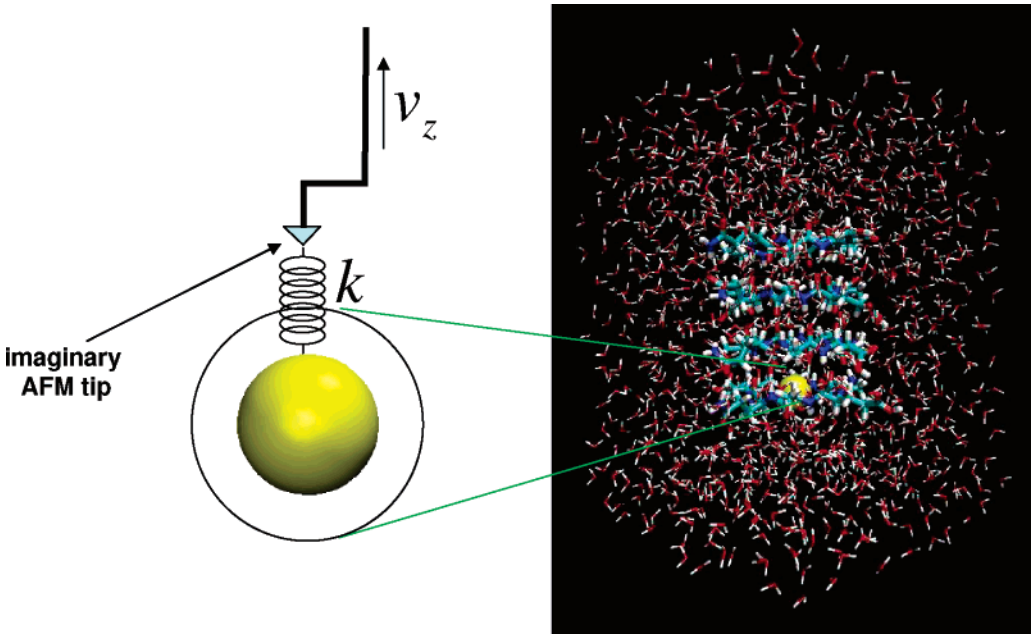


**Figure 2.** A cartoon for a SMD simulation in the present system. An imaginary AFM tip, which is attached to an ion through a harmonic oscillator with spring constant $k$, is being pulled in $\pm z$ direction with a constant pulling velocity $v_z$.

space sum in the Coulomb interaction was evaluated on a grid of $32 \times 32 \times 40$ points. The uniform jelly of charge (or uniform background neutralizing plasma) method was used to neutralize the total cell charge.[36] Although the net charge correction (or volume correction) term[37] due to the interaction of the jelly of charge with each point charge is required in simulations concerning ionic charging free energy,[13,38] the correction term was not taken into account in the current simulations because the term does not affect the PMF obtained from SMD simulations or the dynamics of particles. Van der Waals interactions were truncated at 12 Å and were smoothly switched to 0 from 11 to 12 Å. Because we are interested in the PMF profiles of the ions as a function of the $z$ coordinate but not of the $x$ or $y$ coordinate, the nanotube is constrained in the $z$ direction but moves freely in $x$ or $y$ directions. For this purpose, the α-carbon atoms in the backbone of the cyclic peptide tube were constrained in the $z$ direction with a harmonic spring constant of 20 kcal/mol/Å$^2$. All the simulations were performed with the program NAMD version 2.5,[33] and visualizations were made using the VMD version 1.8.4.[39]

**B. Constant Velocity (cv) SMD Simulations.** The pulling velocity ($v_z$) and the spring constant ($k$) of the harmonic constraint are the most important parameters in the SMD simulation (see Figure 2). To find optimized values for these parameters in the current system, we considered a 1D stochastic model described as[40]

$$m_\nu \frac{\mathrm{d}v_\nu}{\mathrm{d}t} = -\nabla w(z) - \frac{v_\nu}{\beta D_\nu} + f(t) - k(z - v_z t - z_0) \quad (1)$$

where $m_\nu$, $v_\nu$, $D_\nu$, and $z_0$ are the mass, velocity, diffusion coefficient, and initial position of an ion $\nu$, respectively. Also, $\beta$ is $1/(k_B T)$, where $k_B$ is the Boltzmann constant and $T$ is the temperature of the simulation (298 K) and $f(t)$ is a random force acting on the ion. The random force is taken to be Gaussian with zero mean and variance given by

$$\langle f(t) f(t') \rangle = \frac{2}{\beta^2 D} \delta(t - t') \quad (2)$$

For $w(z)$, a periodic PMF, which is assumed to mimic the ion PMF inside the tube, is taken to be

$$w(z) = \frac{w_0}{2}[1 - \cos(2\pi z/L)] \quad (3)$$

where $w_0 = 4.0$ kcal/mol and $L = 4.82$ Å. For this exact PMF curve, we carried out SMD simulations governed by eq 1. The reconstruction of the PMF curves calculated from the SMD simulations was done using a cumulant expansion method[26] that is described in following subsection. The results are presented in Figure 3. Details will be described later, but here, we note that, on the basis of these results, we selected $k = 280$ pN/Å and $v_z = 2.5 \times 10^{-3}$ Å/ps as optimized values for the spring constant and the pulling velocity, respectively, to be used in the nanotube SMD simulations.

Following the work of Jensen et al.,[26] we first divided the nanotube system into ten sections along the $z$ direction and performed SMD simulations in each section independently (see Figure 4a). A single $Na^+$ or $K^+$ ion was inserted at $\pm 11.83$, $\pm 7.12$, and $\pm 2.35$ Å along the $z$-axis, respectively. For the equilibration, the ion is constrained in the $z$ direction with a spring constant of 20 kcal/mol/Å$_2$ at the inserted position. After equilibration, the constraint was lifted and a harmonic constraint with a spring constant of 280 pN/Å was attached to the ion that was pulled in the positive or negative $z$ direction with a constant pulling velocity of $2.5 \times 10^{-3}$ Å/ps (see Figure 2). The system was equilibrated for 1 ns, and the SMD simulation data for the PMF calculation were collected during another 1.2 ns. In the case of ions placed at $z = \pm 11.83$ Å, the ions were pulled toward the entrance of the nanotube from the outside to investigate whether the ions are still bound to the nanotube or not. The fact that all the trajectories of both $Na^+$ and $K^+$ ended up inside the nanotube shows that the ions are still bound to the nanotube at $z = \pm 11.83$ Å. As a result, we did not use a cylindrical constraint to restrain the ion laterally outside the channel.[19,20]

Four SMD simulations in each section were carried out for good statistics. Because it is clear that the PMF profile must be

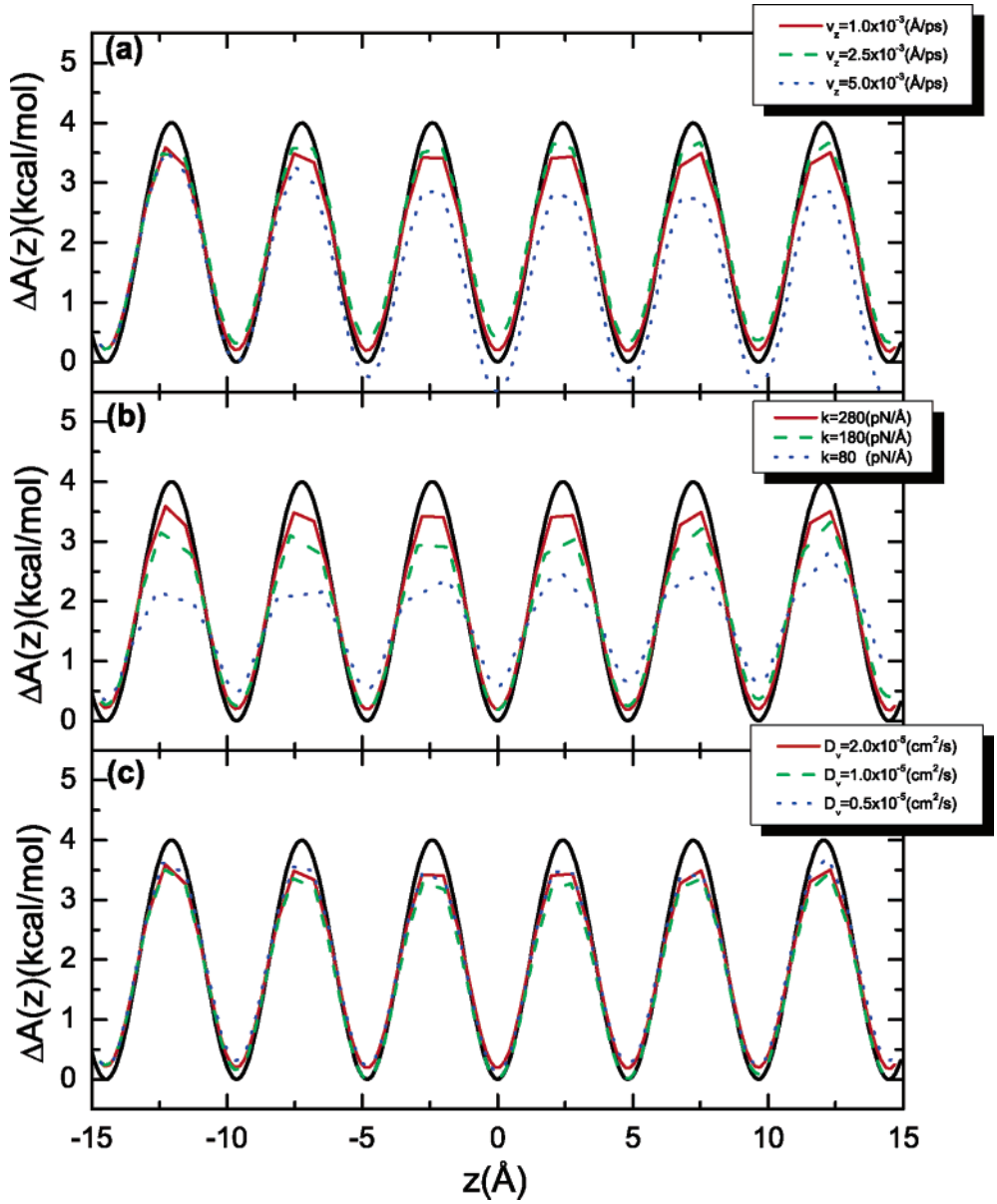


**Figure 3.** PMF reconstructions from SMD simulations for a stochastic model system. The solid black line represents the exact PMF. The dependence of the reconstructed PMF on (a) pulling velocities, (b) the spring constant of the harmonic constraint, and (c) the ion diffusion coefficient are shown. In (a), $k = 280$ pN/Å and $D_v = 2.0 \times 10^{-5}$ cm$^2$/s; in (b), $v_z = 1.0 \times 10^{-3}$ Å/ps and $D_v = 2.0 \times 10^{-5}$ cm$^2$/s; and in (c), $v_z = 1.0 \times 10^{-3}$ Å/ps and $k = 280$ pN/Å.

symmetric due to the symmetry of the nanotube, we averaged the PMF data from the corresponding sections from the middle of the channel to obtain better statistics.

**C. Reconstruction of the PMF from SMD Simulations.** The reconstruction of the PMF from SMD simulations is based on the well-known Jarzynski equality:[29,41,42]

$$\Delta A = -\beta^{-1} \ln\langle \exp[-\beta W] \rangle \tag{4}$$

where $\Delta A$ is a free energy difference and $W$ is the nonequilibrium work. This theorem states that equilibrium properties of a system can be obtained from nonequilibrium processes. Recently, Jensen and co-workers have proposed a PMF reconstruction method from a limited number of SMD simulation trajectories for a channel system.[26] Because the details of the PMF reconstruction method are discussed elsewhere,[25,26,28] we only show some key equations here. The free energy difference between a final state and an initial state can be recast by the second-order cumulant expansion method into[26,28]

$$\Delta A(\langle \bar{z}(j) \rangle) \simeq \langle \bar{W}(j) \rangle - \frac{\beta}{2}[\langle \bar{W}(j)^2 \rangle - \langle \bar{W}(j) \rangle^2] \tag{5}$$

Here, $\langle \bar{z}(j) \rangle = \sum_n \bar{z}_n(j)/N$, where $\bar{z}_n(j) = \int_j \mathrm{d}t\, z[\mathbf{r}_n(t)]/\Delta t$, $n$ is $n$-th trajectory, $j$ is the $j$-th window, $N$ is the number of trajectories in each section, and $\Delta t$ is the width of time windows. Also, $\langle \bar{W}(j)^q \rangle$ is defined as[26]

$$\langle \bar{W}(j)^q \rangle = \frac{1}{N} \sum_n \left\{ \int_j \frac{\mathrm{d}t}{\Delta t} \left[ W_n(t) - \frac{k}{2} ((\langle \bar{z}(j) \rangle - z_0 - v_z \bar{t}(j))^2 \right] \right\}^q \tag{6}$$

where $\bar{t}(j) = \int_j \mathrm{d}t/\Delta t$, $z_0$ is the initial position of the ion, $k$ is the spring constant of a harmonic constraint attached to the ion,

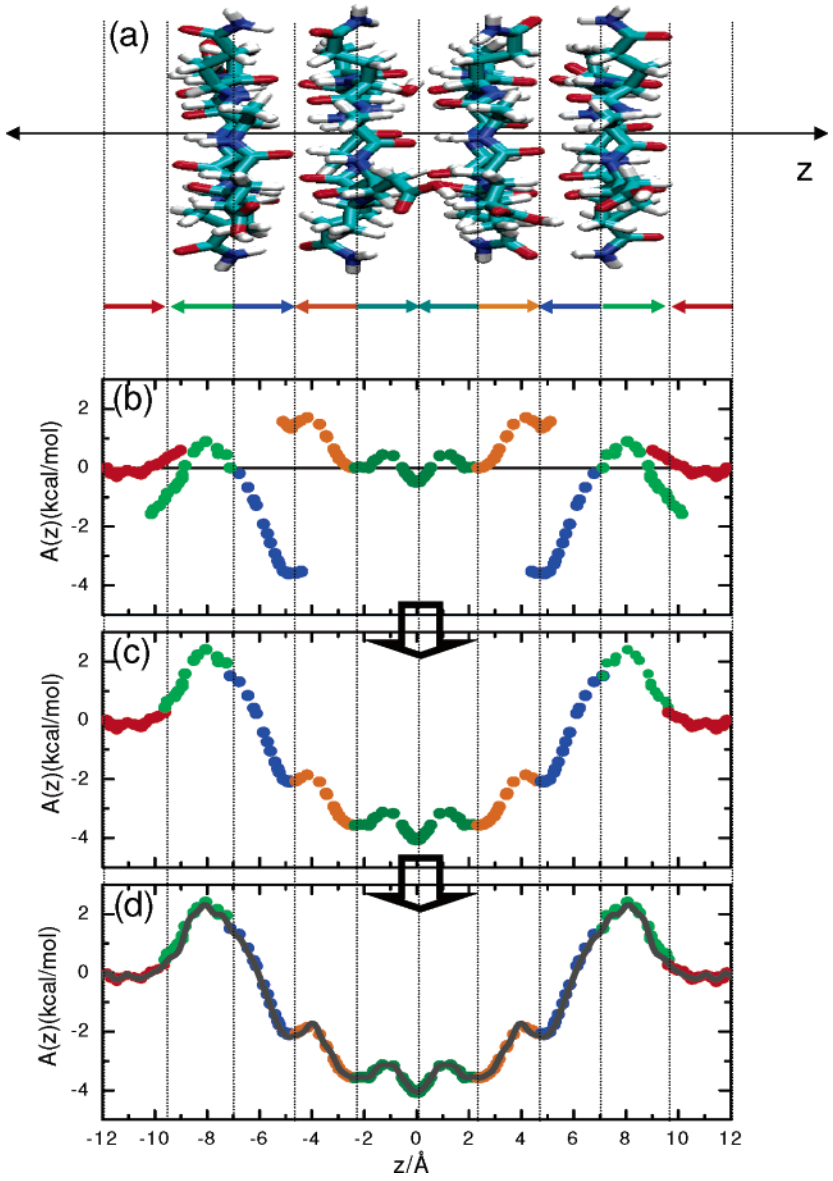


**Figure 4.** PMF reconstruction procedure. (a) Cyclic peptide nanotube divided by 10 sections. The arrows show the direction of the pulling velocity in each section. (b) PMF profiles reconstructed in each section before matching. (c) PMF profile reconstructed after matching. (d) Reconstructed PMF and the symmetric function in eq 9 (dark gray) used for the reconstruction.

$\upsilon_z$ is a pulling velocity in the $z$ direction, and $W_n(t)$ is the external work in the $n$-th trajectory. This work is defined as[26]

$$W_n(t) = -k\int_0^t \mathrm{d}t'\ \upsilon_z\{z[\mathbf{r}_n(t')] - z_0 - \upsilon_z t']\} \qquad (7)$$

As mentioned above, we divided the cyclic peptide nanotube into ten sections and performed the cv-SMD simulations independently through each section. Each sectional PMF profile was assembled first by using a matching relation:[22]

$$P_2'(z) = P_2(z) \times \frac{P_1(z_a)}{P_2(z_b)} \qquad (8)$$

where $z_a \approx z_b$ and $P_i(z)$ and $P_i'(z)$ are distribution functions before and after matching. These are given by $P_i(z) \propto \exp^{-\beta} w_i(z)$ where $w_i(z)$ is the PMF of the $i$-th section before matching. The final PMF was reconstructed by further minimizing the sectional mismatch using a linear combination of $M$ (= 40) symmetric functions:

$$\tilde{A}(z) \equiv \sum_{m=1}^{M} a_m \sin^2[m\pi(z - z_i)/(z_f - z_i)] \qquad (9)$$

where $z_i$ and $z_f$ are −11.83 and 11.83 Å, respectively. See ref 26 for details. Figure 4b and c show the PMF profiles in each section before and after matching. The optimized function in eq 9 is presented in Figure 4d.

## III. Data and Results

**A. PMF Profiles for the Stochastic Model System.** Figure 3a shows the dependence of the PMF profiles reconstructed from cv-SMD simulations for the stochastic model system, considering the effect of the pulling velocity ($\upsilon_z$). Because of a long relaxation time to equilibrium, a larger pulling velocity makes the process more irreversible and the average external work done

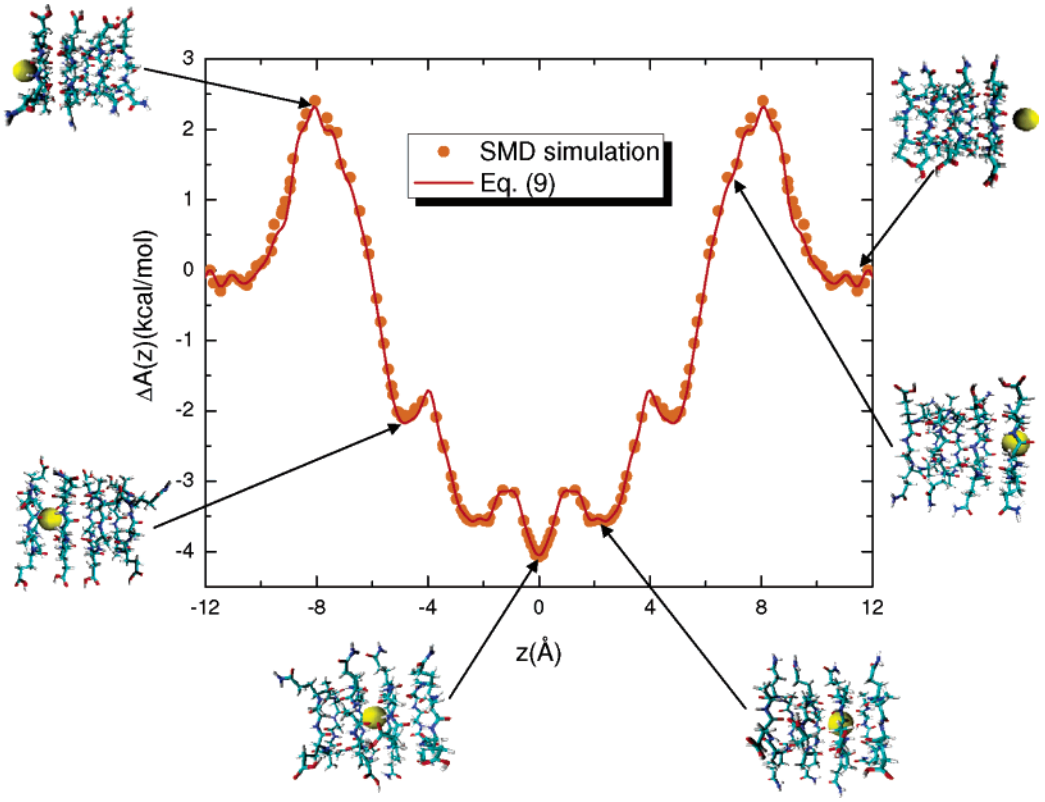


**Figure 5.** $Na^+$ PMF profile. $Na^+$ positions corresponding to $z$ coordinates along the cyclic peptide nanotube are also shown in the inserted snapshots.

on the system becomes larger than the free energy difference.[29] Due to the exponential nature of eq 4 and the limited number of samplings, this forces the reconstructed PMF to be far from the exact PMF.[27]

The position fluctuation associated with a spring constant $k$ connecting between the ion and the imaginary AFM tip can be described using[40]

$$\delta z \sim \sqrt{k_B T/k} \tag{10}$$

The use of a soft spring causes a large fluctuation in the position and makes it difficult to estimate the fine structure of the PMF. To avoid this difficulty, the SMD simulation uses the stiff-spring approximation, which assumes that the spring constant must be sufficiently large that the ion closely follows the tip.[27] The effect of spring stiffness on the PMF is shown in Figure 3b. This clearly shows that the reconstructed PMF profiles digress more from the exact PMF as the spring constant gets softer.

Another factor that affects the PMF reconstruction from the cv-SMD is the diffusion coefficient or friction coefficient of the ion. As the diffusion coefficient decreases (or the friction coefficient increases), the energy dissipation from the ion to the bath increases and the process gets irreversible more quickly. This also leads to bad sampling in the PMF reconstruction. Figure 3c shows the results from three different ion diffusion coefficients that represent the values in bulk ($2.0 \times 10^{-5}$cm$^2$/s) and estimates for ion channels ($1.0 \times 10^{-5}$–$0.5 \times 10^{-5}$cm$^2$/s).[19,20] It appears that diffusion coefficients in the indicated range have little effect on the reconstructed PMF profiles.

**B. PMF Profile of a Single $Na^+$ Ion from cv-SMD Simulations.** Figure 5 shows the PMF profile for a single $Na^+$ moving through the cyclic peptide nanotube. The positions of the ion in the cyclic peptide nanotube are also shown in several places. Several features in the PMF profile are worth addressing. First of all, energy barriers of ~2.4 kcal/mol show up at the both entrances to the nanotube ($z = \pm 8.0$ Å). These energy barriers, so-called dielectric barriers, dielectric self-energy barriers, or desolvation penalties, appear because several water molecules that surround the $Na^+$ ion are removed for the ion to enter the mouth of the nanotube. Many studies have been done to calculate the dielectric barrier energies in ion channels.[43−46] Beckstein et al. used PB equations and MD simulations to obtain free energy profiles inside model ion channels with no fixed charges and radii varying from 1.5 to 10.0 Å. The barrier heights they obtained from the MD simulations ranged from 24 ($r$ = 1.5 Å) to 2.5 kcal/mol ($r$ = 10.0 Å).[46] Cyclic peptide nanotubes have negatively charged carbonyl oxygens on the backbone, and there are strong attractive interactions between cations and the carbonyl oxygens.[17] Consequently, the energy barriers at the channel entrances are a combined result of the desolvation penalty and the attractions between $Na^+$ and the carbonyl oxygens. As mentioned in Section II.B, $Na^+$ at $z = \pm 11.83$ Å is still bound to the cyclic peptide. If the ion is pulled from bulk toward the entrance of the tube, the dielectric barrier must be higher than the 2.4 kcal/mol value we obtained. Second, the well depth of the PMF profile is −4.1 kcal/mol, which is smaller than the −11.8 kcal/mol value predicted using a free energy perturbation calculation for a model cyclic peptide nanotube by Asthagiri and Bashford.[13] Note that their work determined only the electrostatic component of the free energy; in contrast, our study calculated the total free energy, so the direct comparison of their results and ours cannot be made. Also note that Asthagiri and Bashford did not study other aspects of the PMF in their work. So, the presence of barriers at the nanotube entrances was not determined previously. Third, our results show that there are small barriers and wells in the PMF curve, which suggest that the $Na^+$ ion diffuses through the peptide nanotube with a series of hoppings. A similar hopping mechanism for water molecules diffusing inside the peptide nanotube was found in MD simulations.[12]

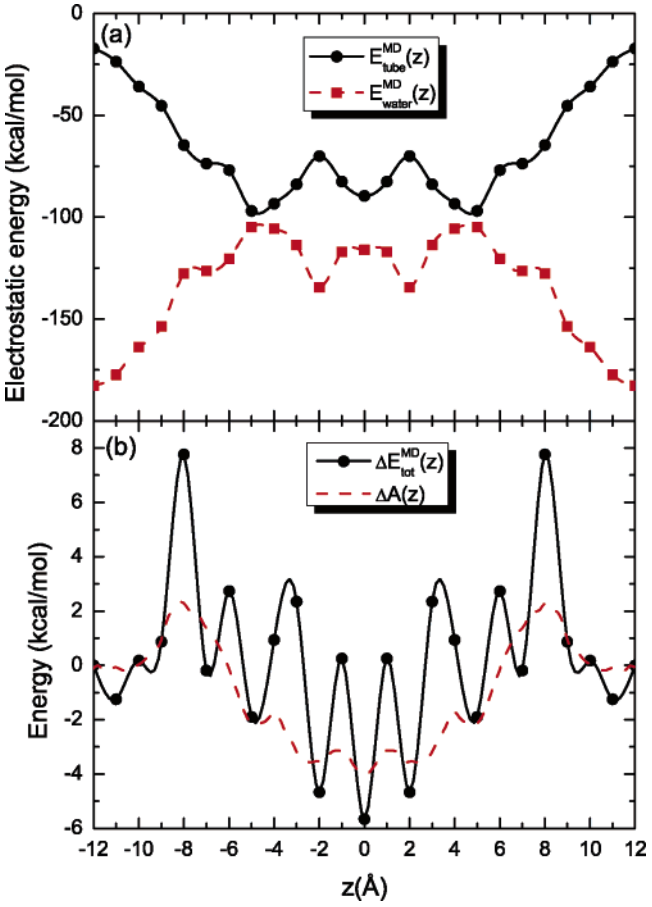


**Figure 6.** (a) Electrostatic interaction energies of $Na^+$ with the tube ($E^{MD}_{tube}(z)$) and with the water ($E^{MD}_{water}(z)$). (b) Comparison between the total electrostatic interaction energy difference ($\Delta E^{MD}_{tot}(z)(a)$) and the PMF ($\Delta A(z)$). A single $Na^+$ is fixed at −12.0, −11.0, −10.0, ..., 0.0 Å. The results were duplicated along the positive *z*-axis by assuming that they should be the same by symmetry. The curves were smoothed with a spline method.

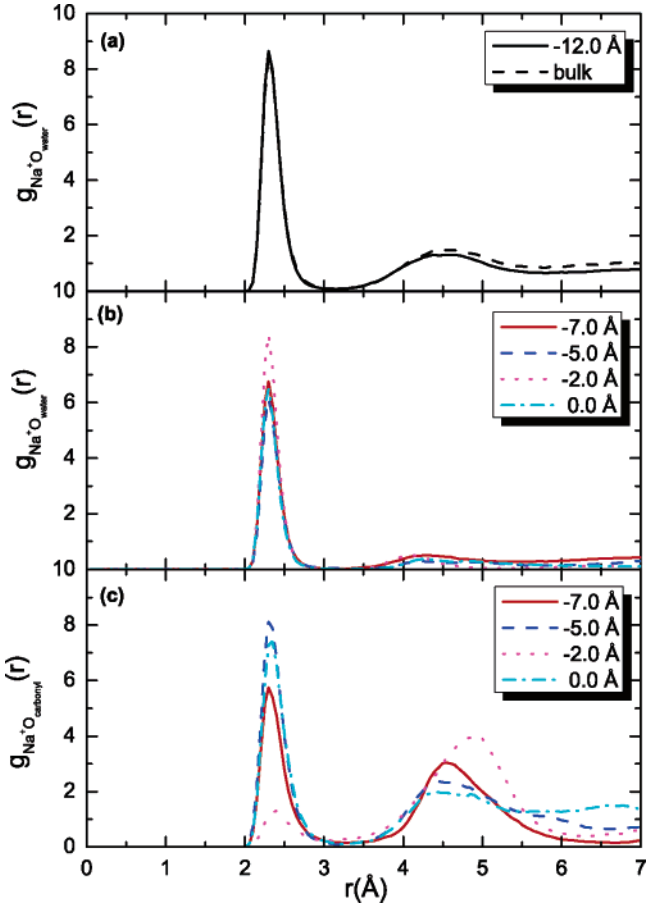


**Figure 7.** RDF between $Na^+$ and the water oxygens or between $Na^+$ and the carbonyl oxygens for several $Na^+$ positions. The simulations are the same as in Figure 6. A $Na^+$ is fixed at −12.0, −11.0, −10.0, ..., 0.0 Å. Parts (a) and (b) show the RDFs between the $Na^+$ and water oxygens. (c) RDFs between the $Na^+$ and the carbonyl oxygens on the cyclic peptide nanotube. In (c), the scale of $g_{Na^+O_{carbonyl}}(r)$ is arbitrary.

The electrostatic interactions of a $Na^+$ with the cyclic peptide nanotube and water are investigated in Figure 6a. Simulations of 2.0 ns with a time step of 2.0 fs were performed with a $Na^+$ ion fixed at −12.0, −11.0, −10.0, ..., 0.0 Å. The first 1.0 ns was for the equilibration, and the other 1.0 ns was for the data collection. Entering deep into the middle of the nanotube, the $Na^+$ is stabilized due to electrostatic interaction with the carbonyl oxygens, but the desolvation penalty increases due to the removal of some water molecules in the solvation shell. The two energy wells in the $E^{MD}_{water}(z)$ show that the $Na^+$, which is positioned at the α-plane regions ($z = \pm 2.0$ Å), can interact more with water molecules that reside in the midplane regions at both sides of the α-plane region. The two energy barriers in the $E^{MD}_{tube}(z)$ suggest that, due to strong interaction of the $Na^+$ with water molecules in the α-plane region ($z = \pm 2.0$ Å), the ion interaction with the carbonyl oxygens is weaker. Figure 6b shows the contribution of the electrostatic interaction energy to the PMF where $\Delta E^{MD}_{tot}(z)$ is defined as

$$E^{MD}_{tot}(z) = E^{MD}_{tot}(z) - E^{MD}_{tot}(\pm 12.0\ \text{Å}) \qquad (11)$$

where $E^{MD}_{tot}(z) = E^{MD}_{tube}(z) + E^{MD}_{water}(z)$. The difference between the total electrostatic interaction energy ($\Delta E^{MD}_{tot}(z)$) and the PMF ($\Delta A(z)$) indicates that there are also the contributions from other intra- and intermolecular interaction energies and the entropy of the system to the PMF.

Figure 7 shows the radial distribution functions (RDF) between a $Na^+$ ion and either water oxygens or carbonyl oxygens for several $Na^+$ positions. The first solvation shell radius, which is defined as the first minimum in $g_{Na^+O_{water}}(r)$, is determined as 3.1 Å from Figures 7a and b. This value is similar to that obtained in other studies.[47,48] The first peak in the RDF in Figure 7a is almost like that of the bulk RDF, which implies that the $Na^+$ is far enough from the cyclic peptide nanotube to have a bulk-like first peak and is well solvated by water molecules in the first solvation shell at −12.0 Å. The second peak is lower than in bulk because there are a smaller number of water molecules between the ion and the channel entrance. In Figure 7b, the first peak of $g_{Na^+O_{water}}(r)$ for a $Na^+$ location of −2.0 Å is the highest among those plotted because the position −2.0 Å corresponds to the α-plane region and on both sides of that α-plane there are midplanes that accommodate more water molecules.[12] Although the −7.0 Å position also corresponds to the α-plane region, the first peak is not as high as at −2.0 Å because access of the water molecules to the channel entrance from outside the tube is slightly prohibited by the dangling carbonyl groups and the side chains of the cyclic peptide rings at the end. When the $Na^+$ is located at 0.0 or −5.0 Å, it is at the midplane regions. Because the number of water molecules at the α-plane regions on both sides of the midplane region is smaller, the first peaks at the midplane regions are lower. Figure 7c shows that $g_{Na^+O_{carbonyl}}(r)$ has two peaks positioned at around 2.3 and 4.7 Å. The first peak at 2.3 Å arises from interactions

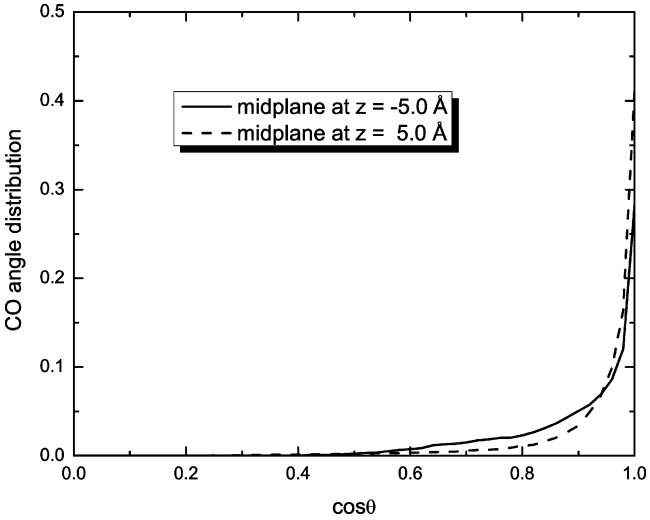


**Figure 8.** The angle distribution of the eight carbonyl groups closest to a $Na^+$ ion placed at $z = -5.0$ Å. For comparison, the angle distribution of the eight carbonyl groups in a midplane at $z = 5.0$ Å are also shown. The angle distribution was normalized. For the definition of cos $\theta$, see eq 12.

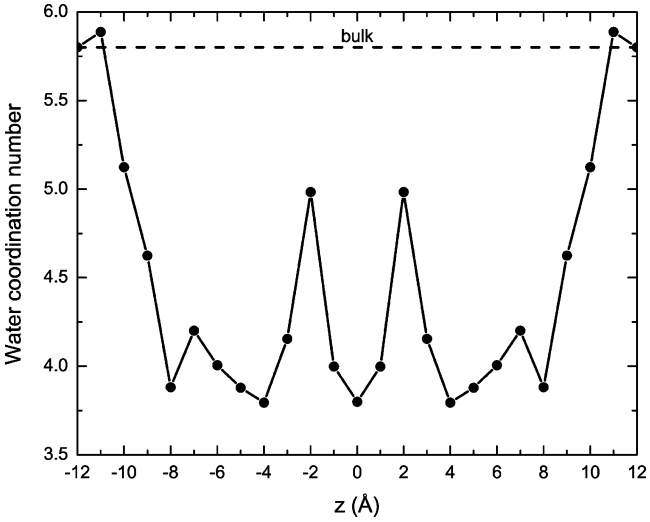


**Figure 9.** The water coordination number in the first solvation shell around $Na^+$. The first solvation shell radius is determined as 3.1 Å. The simulations are the same as in Figure 6.

between the $Na^+$ and carbonyl oxygens that move relatively freely in the backbone. The second peak location at 4.7 Å coincides with the radius of the cyclic peptide nanotube, as is known from the experiments.[5] This indicates that the second peak appears as a result of the interaction of $Na^+$ with carbonyl oxygens that are relatively rigid and make more contributions to hydrogen bonding for the self-assembling of the peptide nanotube. It should be noted that $g_{Na^+O_{carbonyl}}(r)$ for the $-2.0$ Å location has the smallest peak because the $Na^+$ at that position has the strongest interaction with water and the carbonyl oxygens protrude above and below the α-plane by 1.7 Å. This protrusion makes the interaction of an ion with the carbonyl oxygens unfavorable when the ion sits in the α-plane.

The angle distributions of the carbonyl groups (C═O) on the backbone of the tube around a $Na^+$ ion are investigated in Figure 8. Here, the angle $\theta$ is defined as

$$\cos\theta = \left|\frac{\vec{r}_{OC}\cdot\hat{z}}{|\vec{r}_{OC}||\hat{z}|}\right| \tag{12}$$

where $\vec{r}_{OC} = \vec{r}_O - \vec{r}_C$ and $\hat{z}$ is a unit vector parallel to the tube axis. High cosine values (= low angles) mean that the carbonyl groups are parallel to the *z*-axis and are mostly participating in hydrogen bonding. In the simulation, one $Na^+$ ion is placed at a midplane region, $z = -5.0$ Å, and the angle distribution of the eight carbonyl groups closest to the ion are calculated. For comparison, the angle distribution of the eight carbonyl groups in a midplane region at $z = 5.0$ Å in the same simulation are also examined. Figure 8 shows sharp peaks at around $\theta = 0$ because the carbonyl groups are mostly participating in hydrogen bonding to maintain the tubular structure of the cyclic peptide nanotube. There are also long tails that indicate the orientational fluctuation of the carbonyl groups. The sharp peak suggests that the carbonyl groups in the cyclic peptide nanotube are relatively rigid compared with the dynamic carbonyl groups observed in the selectivity filter of the KcsA channel.[49] The carbonyl groups in the midplane region where the $Na^+$ is placed have a little broader distribution than for regions without the ion. This implies that the $Na^+$ ion can slightly alter the orientation of the carbonyl groups. It should be noted that the rigidity of the carbonyl groups can be partially attributed to the constraints applied to the α-carbon atoms in the backbone of the cyclic peptide.

Figure 9 shows the coordination number of water molecules in the first shell around a $Na^+$ that is fixed at $-12.0$, $-11.0$, $-10.0$, ..., 0.0 Å. To obtain the coordination number in the first shell, the first solvation shell radius of 3.1 Å obtained from RDF curves in Figure 7a and b was used. The figure shows that, as a $Na^+$ ion approaches the entrance of the nanotube, approximately two water molecules are removed from the ion. This desolvation cost appears as the dielectric energy barriers shown in Figure 5. The two peaks at ±2.0 Å (α-plane regions) indicate that five water molecules surround the $Na^+$ ion at that location, and this relatively stronger solvation leads to the energy wells in $A(z)$ in Figure 5 and in $E^{MD}_{water}(z)$ in Figure 6a.

A typical configuration of a single $Na^+$ ion and the water molecules in the first solvation shell at a midplane site ($z = 0.0$ Å) is shown in Figure 10a. As Engels et al. indicated,[12] there are two coordinating water molecules in the midplane and one water molecule in each α-plane region so that the coordination number is approximately four. As shown in Figure 10b, when a $Na^+$ is positioned at $z = -2.0$ Å (an α-plane zone), the ion is surrounded by five water molecules of which three are located in one midplane region and two in the other midplane region. This explains why the energy wells appear at $z = \pm 2.0$ Å in $E^{MD}_{water}(z)$ in Figure 6a. In that position, the ion is relatively well solvated and stabilized by five water molecules. At the entrance to the channel, as shown in Figure 10c, five water molecules are surrounding the $Na^+$, but one water molecule does not interact with the ion strongly. This weak interaction can be attributed to the dangling carbonyl groups and the side chains in the cyclic peptide rings at the end that are not as rigid as the interior rings. The dangling carbonyl groups in the end ring can interact more strongly with the ion, and as a result, the interaction of the ion with water molecules is reduced.

The significance of the SMD calculation of the PMF can be demonstrated by comparing it with the electrostatic energy that is obtained from the PB equation, a continuum dielectric model. To generate the latter, at each position of $Na^+$ along the *z*-axis, the electrostatic energy from the reaction field, $\Delta E^{PB}_{rfd}(z)$, as well as from the fixed charges in the cyclic peptide nanotube,

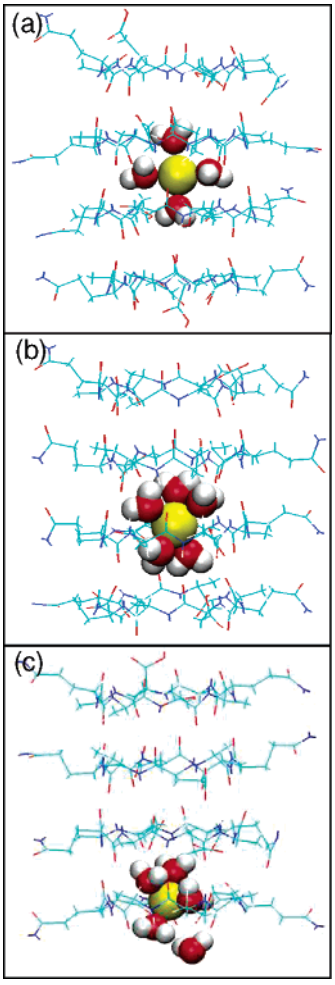


**Figure 10.** Typical ion and water configurations inside the cyclic peptide nanotube at $Na^+$ positions of (a) 0.0 Å (midplane), (b) −2.0 Å (α-plane), and (c) −7.0 Å (channel entrance).

$\Delta E^{PB}_{tube}(z)$, are computed. The total electrostatic energy, $\Delta E^{PB}_{tot}(z)$, is then calculated as

$$\Delta E_{tot}(z) = \Delta E^{PB}_{tube}(z) + \Delta E^{PB}_{rfd}(z) \quad (13a)$$

$$= q_{ion}\phi_{tube}(z) + \frac{1}{2} q_{ion}\phi_{rfd}(z) \quad (13b)$$

in which $q_{ion}$ is an ion charge, $\phi_{tube}(z)$ is the electrostatic potential from the fixed charges in the peptide nanotube, and $\phi_{rfd}(z)$ is the reaction field acting on the ion due to dielectric boundaries between water and the protein. The relative dielectric constant of the cyclic peptide nanotube was chosen as 4.0 in this calculation. The dielectric constant of water inside the ion channel is known to be lower than the bulk value.[45] To obtain the inside-water dielectric coefficient, we assume the simple equation:

$$\epsilon(z) = (\epsilon_{blk} - 1.0)f(z) + 1.0 \quad (14)$$

where the bulk water dielectric constant $\epsilon_{blk}$ is set to 80.0 and $f(z)$ is given by fitting the fraction to the bulk water coordination number from Figure 11a with the function

$$f(z) = \frac{1}{N}\left(a_2 + \frac{a_1 - a_2}{1.0 + e^{-(|z|-z_0)/dz}}\right) \quad (15)$$

where $a_1 = 1.0171$, $a_2 = 0.7066$, $z_0 = 9.7206$, dz = 0.5232,

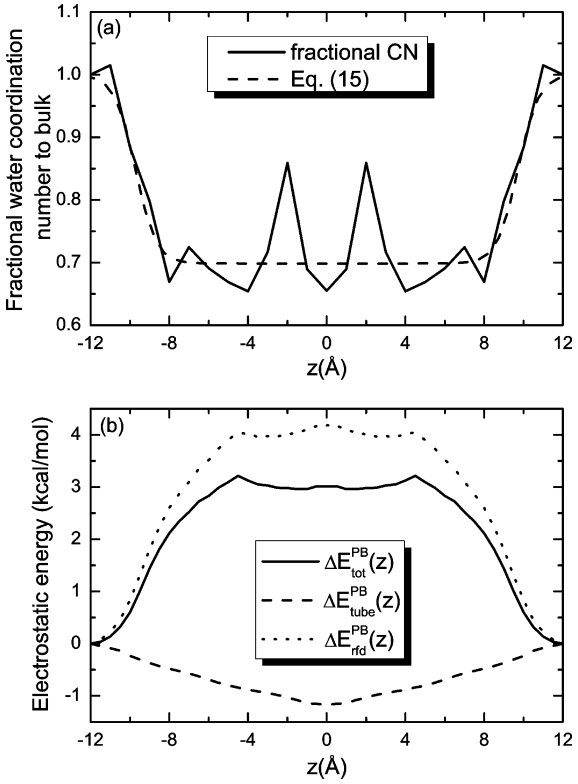


**Figure 11.** (a) Fractional water coordination number around a $Na^+$ inside the cyclic peptide nanotube, referenced to bulk coordination, along with the fitting function in eq 14. (b) Electrostatic energy calculations for $Na^+$ inside the nanotube based on the PB equation. The energy-minimized structure was used for the PB calculations.

and $N$ is a normalization constant. In general, the local dielectric constant of water in an inhomogeneous region depends on the orientation of water molecules and it can be obtained using statistical mechanics.[50−52] In this work, however, we take the local dielectric constant of water to be proportional to the average number of water molecules inside the first solvation shell around an ion. Then the electrostatic potential energy can be obtained by placing the cation in the ion-accessible *xy*-plane at a fixed $z$ position, summing all the electrostatic potential energies in that plane and averaging them. In this way, the size effect of the cation is taken into account.

Figure 11b shows the electrostatic potentials calculated by the PB equation with the water dielectric constant given in eq 14. In contrast with the energy well in the PMF calculation from the SMD simulations in Figure 5 or the electrostatic energies in Figure 6, the PB results predict an energy barrier of 2.6 kcal/mol in the middle of the peptide nanotube. This kind of observation was also made by Asthagiri and Bashford when they obtained the solvation free energy by performing continuum dielectric calculations (PB equation).[13] This indicates that the continuum dielectric model breaks down in a confined region such as a cyclic peptide nanotube and suggests that approaches at the atomic level for water molecules inside cyclic peptide nanotubes are required.

**C. PMF Profile for a Single $K^+$ Ion from cv-SMD Simulations and Comparison with the PMF Profile for $Na^+$.** The PMF curve for a single $K^+$ ion is presented and compared with that for a $Na^+$ in Figure 12. This shows that the PMF calculation for $K^+$ has the same dielectric barrier energy of 2.3 kcal/mol as for $Na^+$, located at the channel entrances ($z = \pm 8$ Å). Also, there are energy wells in the midplane regions ($z =$ 0.0 and ±5.0 Å). However, in contrast to $Na^+$, the PMF does

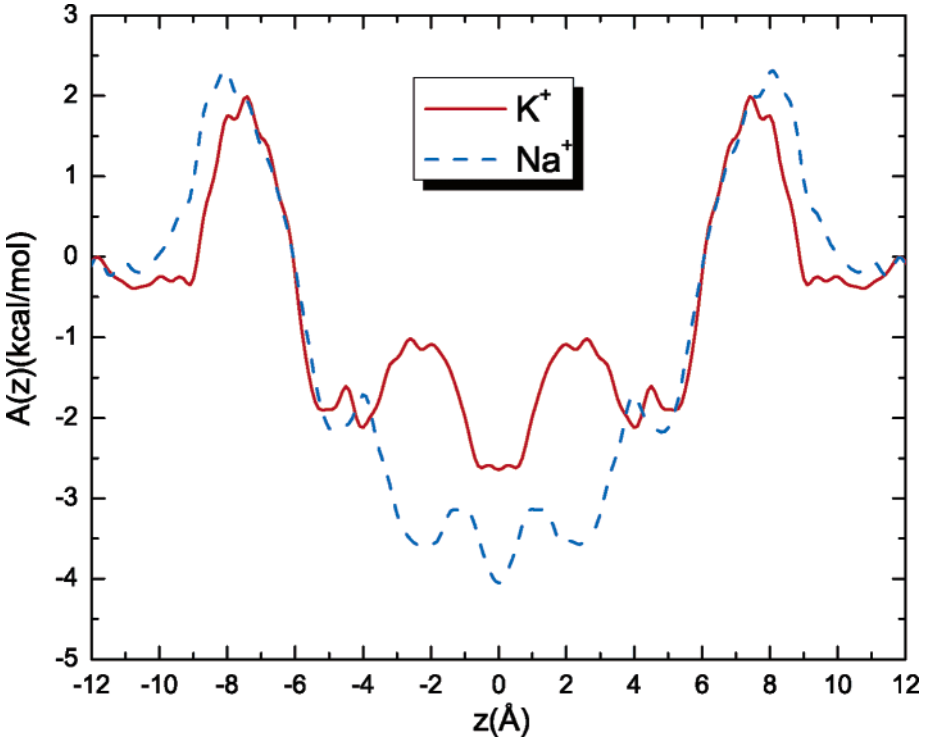


**Figure 12.** Comparison of PMF results for $K^+$ and $Na^+$.

not show energy wells at $z = \pm 2.3$ Å. Also, the energy well in the middle of the $K^+$ PMF profile is higher than the $Na^+$ PMF.

Figure 13a shows a comparison of the electrostatic interaction energies for a $K^+$ with a $Na^+$ ion inside the cyclic peptide nanotube. $E^{MD}_{water}(z)$ for both $K^+$ and $Na^+$ shows increasing electrostatic interaction energies as the nanotube is entered due to desolvation. In addition, there is net attractive interaction between the ions and the carbonyl oxygens in the nanotube. Although $E^{MD}_{tube}(z)$ for both ions has a similar magnitude, the magnitude of $E^{MD}_{water}(z)$ for the two ions is quite different. The close similarity in the $E^{MD}_{tube}(z)$ profiles for the two ions is because both of them are monovalent cations and the radius difference between the two ions is small. As for $E^{MD}_{water}(z)$, the large difference is ascribed to the effect of the bulk solvation free energies. These were calculated in the MD simulations as $-81.5$ kcal/mol for $K^+$ and $-102.6$ kcal/mol for $Na^+$ ion.[35] Comparison of the PMF with the total electrostatic interaction energy difference ($\Delta E^{MD}_{tot}(z)$) is presented in Figure 13b. As mentioned above, the difference between the two comes from the other intra- and intermolecular interaction energies and the entropy of the system.

In Figure 14a, we see that the $g_{K^+O_{water}}(r)$ of the $K^+$ ion at $z = -12$ Å is similar to that in bulk except at long distance, which implies that the $K^+$ cation is well solvated, at least in the first solvation shell. The positions of the peaks in $g_{K^+O_{water}}(r)$ inside the nanotube are nearly the same, but the heights of the peaks are different depending on the locations of the ion, namely the midplanes ($-0.0$ and $-5.0$ Å) or the α-planes ($-2.0$ and $-7.0$ Å). Figures 14b and c show that when the peak of $g_{K^+O_{water}}(r)$ increases, the peak of $g_{K^+O_{carbonyl}}(r)$ decreases due to the competitive interaction of the $K^+$ with the two kinds of oxygens.

Figure 15 shows the angle distributions of the eight carbonyl groups closest to the $K^+$ ion placed at $z = -5.0$ Å. As was the case for the $Na^+$ ion, the carbonyl groups do not show significant deviations from their rigid, close to linear values, indicating the importance of their participation in hydrogen bonding to maintain the tubular structure of the cyclic peptide nanotube. As mentioned in the case of $Na^+$, the rigidity of the carbonyl groups can also be partially attributed to the constraints applied to the α-carbon atoms in the backbone of the cyclic peptide.

The water coordination number of a $K^+$ ion in the first shell is shown in Figure 16. In this calculation, the first solvation shell radius is set as $r_{min} = 3.55$ Å on the basis of Figures 14a and b.[47,53] The water coordination number profile clearly shows why there is no well in the $K^+$ PMF for $z = \pm 2.0$ Å (in the α-plane). Although a $Na^+$ at $z = \pm 2.0$ Å is solvated well enough to give an energy well, a $K^+$ ion is not as well solvated compared to bulk solvation and no energy wells are formed. The smaller solvation of the $K^+$ compared with the $Na^+$ can be ascribed to a smaller solvation free energy for the $K^+$ ion.[35]

Three snapshots of the $K^+$ at $z = 0.0$, $-2.0$, and $-7.0$ Å are shown in Figure 17. It turns out that the interaction of a $K^+$ with water molecules inside the cyclic peptide nanotube is not as strong as that of a $Na^+$ because of the smaller solvation free energy. As a result, a smaller number of water molecules are found around a $K^+$ ion than a $Na^+$. At the midplane in Figure 17a, four water molecules are found around the $K^+$, but one water molecule is loosely bound to the ion. Figure 17b shows that only four water molecules surround the $K^+$ at the α-planes. Due to the dangling carbonyl oxygens and the freely moving side chains of the cyclic peptide ring at the mouth of the tube, water molecules just outside the tube cannot interact with the ion strongly and only one water molecule is shown outside the tube.

The electrostatic energy of a $K^+$ ion inside the cyclic peptide nanotube based on the PB equation is shown in Figure 18b. The position-dependent dielectric constant inside the tube was calculated in the same way as in the case of $Na^+$, and the function $f(z)$ for the $K^+$ is shown in Figure 18a. The parameters used in the function $f(z)$ for the $K^+$ are $a_1 = 1.0173$, $a_2 = 0.5570$, $z_0 = 9.7707$, and $dz = 0.9884$. Included in Figure 18b are comparisons of the $K^+$ and $Na^+$ electrostatic interaction energies based on the PB equation. As in the MD results in Figure 13a, the PB equation predicts almost the same interaction energy of

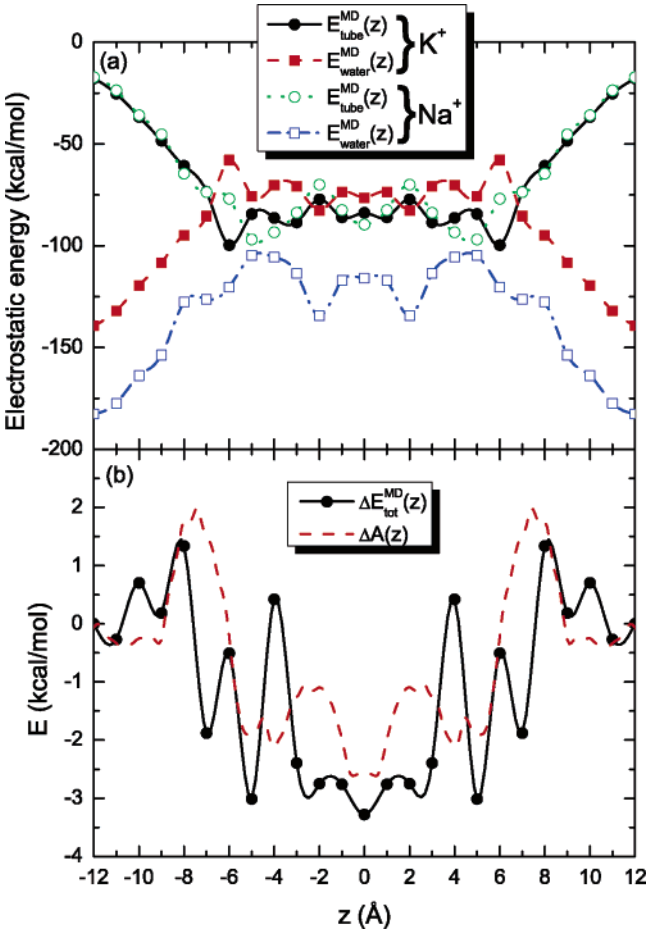


**Figure 13.** (a) Comparisons of the electrostatic interaction energies for $K^+$ and $Na^+$. (b) Comparison between the total electrostatic interaction energy difference ($\Delta E_{tot}^{MD}(z)$) and the PMF ($\Delta A(z)$) for the $K^+$ ion. The simulations are the same as in Figure 6 except for switching $Na^+$ to $K^+$.

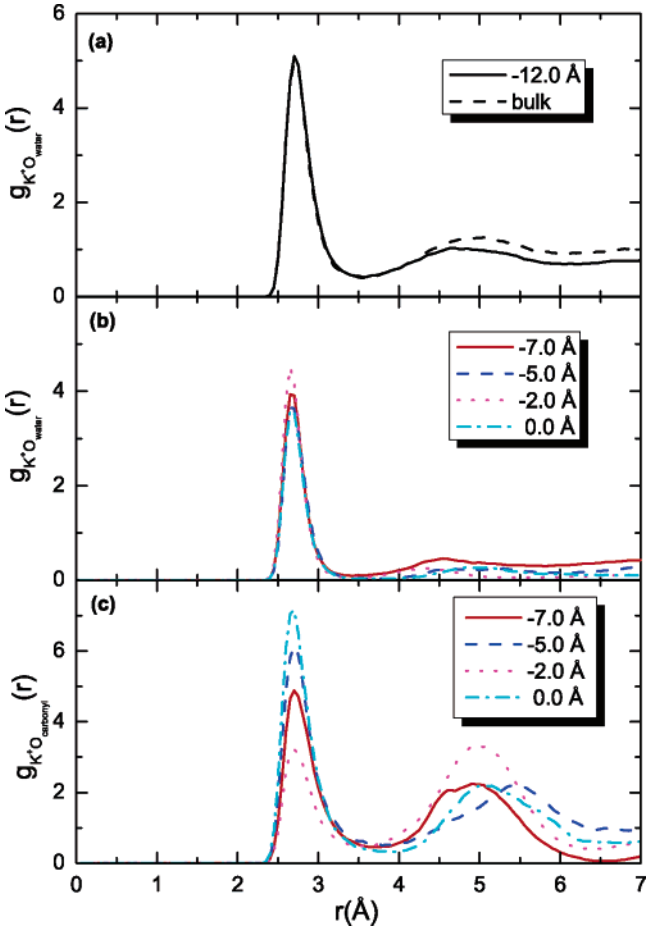


**Figure 14.** RDFs between a $K^+$ and water oxygens and between $K^+$ and the carbonyl oxygens, for several $K^+$ positions. The simulations are the same as in Figure 6 except for switching $Na^+$ to $K^+$. Parts (a) and (b) show the RDF curves for $K^+$ and the water oxygens. (c) Shows the RDF curve between the $K^+$ and carbonyl oxygens on the cyclic peptide nanotube. In (c), the scale of $g_{K^+O_{carbonyl}}(r)$ is arbitrary

the $K^+$ and $Na^+$ with the fixed charges in the cyclic peptide nanotube in Figure 18b. More water molecules are desolvated from $K^+$ than from $Na^+$ so the dielectric constant is lower for $K^+$. This leads to a higher reaction field energy and therefore higher total energy for $K^+$.

## IV. Discussion and Conclusions

Ghadiri et al. observed a higher $K^+$ conductance (65 pS) than for $Na^+$ (55 pS) for a cyclic peptide nanotube embedded in a membrane bilayer.[6] The comparison of the PMF profiles for a single $Na^+$ and a $K^+$ ion provides insight into the conductance difference between these ions. First, both of them have similar dielectric barriers at the entrances to the cyclic peptide nanotube, suggesting that barrier crossing does not affect the permeability difference. Rather, the permeability difference appears to come from the energy well difference inside the nanotube. Because the $Na^+$ PMF profile has deeper energy wells, $Na^+$ ions can be trapped longer than $K^+$ ions and the mobility of $Na^+$ ions is therefore reduced compared to $K^+$. The same observation was made in an MD simulation study of $K^+$ versus $Na^+$ in a KcsA channel selectivity filter.[54] In that MD simulation study, the slower translocation of $Na^+$ over $K^+$ is attributed to the stronger binding of $Na^+$ to sites within the filter. Figure 13a shows that the interactions of a $Na^+$ and a $K^+$ with the fixed charges in the peptide tube are not much different, but the interactions of the both ions with water molecules are quite different. It suggests that a $Na^+$ ion has more water molecules interacting with it

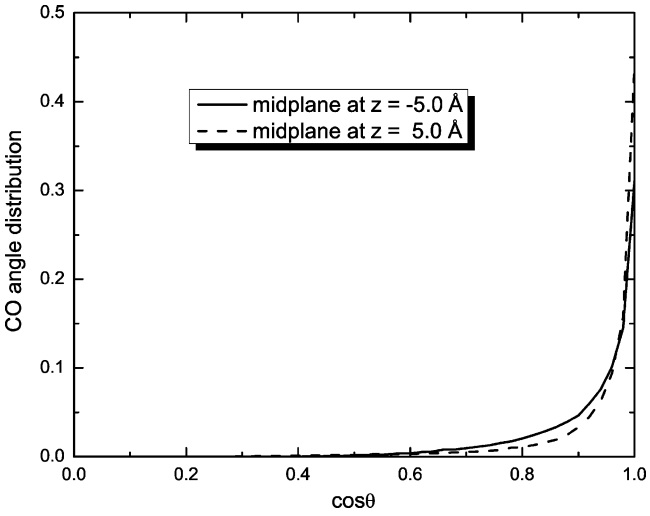


**Figure 15.** Angle distribution for the eight carbonyl groups closest to a $K^+$ ion that is placed at $z = -5.0$ Å, as in Figure 8.

than a $K^+$ ion inside the cyclic peptide nanotube due to a larger solvation free energy of $Na^+$ ions. Consequently, compared with $K^+$ ions, water molecules are more tightly bound to $Na^+$ ions, and this makes $Na^+$ ions slow down inside the tube.

The PMF calculations also show that, in contrast to $K^+$, a $Na^+$ ion can be more stabilized at α-plane regions due to

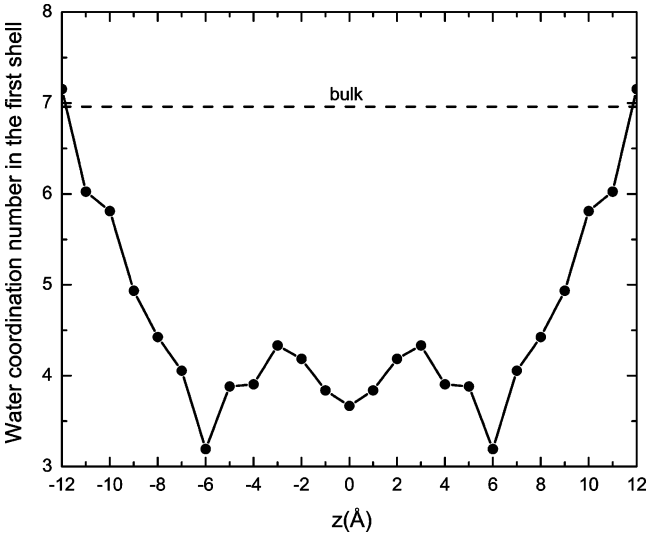


**Figure 16.** The water coordination number in the first solvation shell around $K^+$. The first solvation shell radius is determined as 3.55 Å. The simulations are the same as in Figure 6 except for switching $Na^+$ to $K^+$.

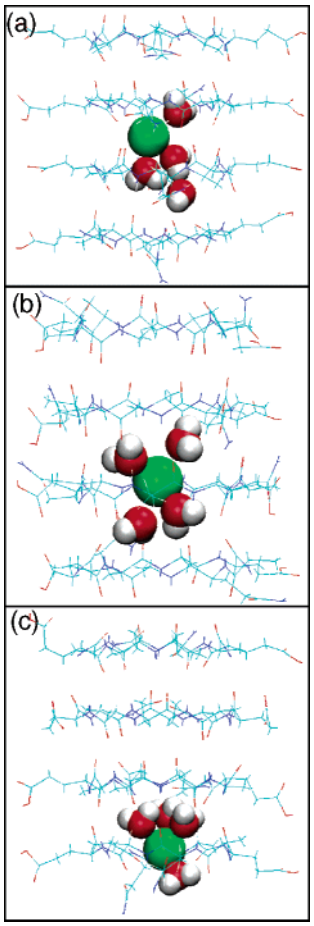


**Figure 17.** Typical ion and water configurations inside the cyclic peptide nanotube for $K^+$ positions of (a) 0.0 Å (midplane), (b) −2.0 Å (α-plane), and (c) −7.0 Å (channel entrance).

favorable solvation with neighboring water molecules located at the midplanes on the both sides of the α-plane. The water coordination number calculations confirm that a $Na^+$ ion at the α-plane regions can be favorably solvated by five water molecules in the first solvation shell. A similar effect of the water solvation shell on preferential transport of $Na^+$ over $Cl^-$

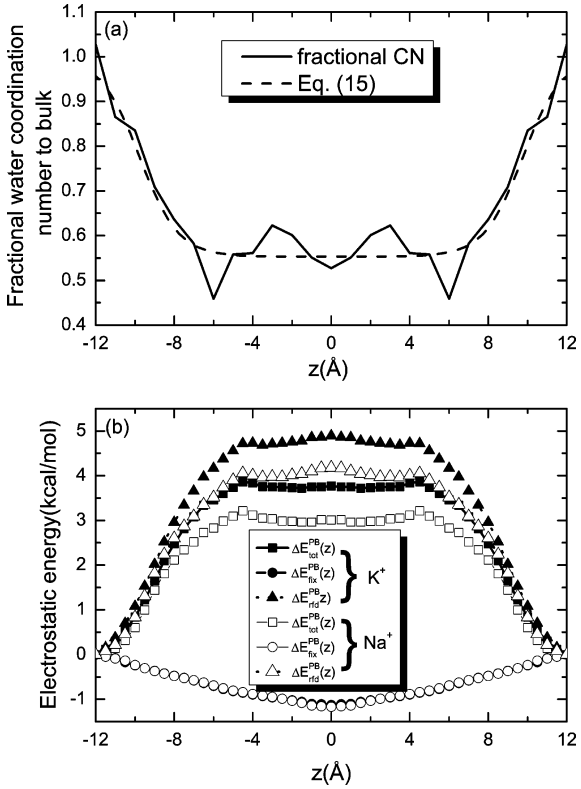


**Figure 18.** (a) Fractional water coordination number for $K^+$ inside the cyclic peptide nanotube along with the fit provided by eq 14. (b) Comparison of electrostatic energies for $K^+$ and $Na^+$ based on the PB equation. The energy-minimized structure was used for the PB calculations.

in a single wall carbon nanotube has been reported by Leung and co-workers.[55]

The PMF and RDF calculations for several locations inside the nanotube shown in Figures 7 and 14 reveal that the interactions of a $Na^+$ and a $K^+$ ion with water and carbonyl oxygens on the backbone of the cyclic peptide nanotube play a key role in the energetics inside the nanotube.[21] First of all, there is competition between water molecules and the carbonyl oxygens for the interaction with ions. The relatively smaller first peak of the $g_{Na^+O_{carbonyl}}(r)$ at the α-plane ($z = -2.0$ Å) compared with the second peak implies that the strong interaction between the $Na^+$ and water molecules prevents the interaction between the ion and the carbonyl oxygens. On the contrary, the same size first and second peaks of $g_{K^+O_{carbonyl}}(r)$ at the α-plane indicate that the $K^+$ interaction with water is not as strong as $Na^+$ and the interaction with the carbonyl oxygens increases.

The angle distribution functions of the carbonyl groups in Figures 8 and 15 suggest that the carbonyl groups are relatively rigid, with only slight alteration of the carbonyl orientation due to nearby ions. This is in contrast with the carbonyl groups observed in the selectivity filter of the KcsA ion channel, which are described as dynamic (or "liquid-like").[49] We ascribe the difference to the fact that, in addition to the interaction with ions, the carbonyl groups in the cyclic peptide nanotube are also participating in hydrogen bonding that maintains the tubular structure whereas the carbonyl groups in the KcsA channel entirely contribute to the interaction with ions. It should be noted, however, that the rigidity of the carbonyl groups can be partially ascribed to the constraints applied to the α-carbon atoms in the backbone of the cyclic peptide.

In our study, the SMD simulation trajectories showed that ions placed at $z = \pm 11.83$ Å are still bound to the channel, and as a result, due to the lack of a proper bulk reference value, the current PMF calculations cannot be directly used to determine the equilibrium binding constant of ions in the tube.

Note that the PMF profiles we have obtained are for a single ion whereas multiple ions are involved in ion conductance measurements. Consequently, PMF calculations for a system with multiple ions are needed to provide a quantitative understanding of ion transport. Calculating such PMF information is a very major undertaking, so it is encouraging that our single ion results show at least a qualitative connection with experiment.

In the actual measurements, the cyclic peptide nanotubes are embedded in a membrane bilayer. This is replaced by water in the current study. PMF calculations for ions inside a cyclic peptide nanotube embedded in a membrane will show the effect of the membrane on PMF profiles when compared with a PMF profile for ions inside a tube in aqueous conditions.

The calculation of water coordination number inside the nanotube suggests that the properties of water inside the tube should be different from bulk water. In addition, our study shows that the dynamics of ions inside the cyclic peptide nanotube are quite different from ions in bulk due to the interaction with the carbonyl groups and water in the tube. Consequently, the computation of the water dielectric constant and the ion diffusion coefficient in a cyclic peptide nanotube will help understand the dynamics of water and ions in a confined region and its influence on ion conductance.

Umbrella sampling is a popular method for obtaining the PMF. The comparison of the PMF calculation from the SMD simulation with that from umbrella sampling will help verify the accuracy of the present PMF calculations.

**Acknowledgment.** This work was supported by the Network for Computational Nanotechnology (NCN) through a grant from the National Science Foundation. This work was partially supported by the National Center for Supercomputing Applications (NCSA) utilizing the NCSA Tungsten Cluster. We thank Reza Ghadiri for helpful suggestions.

## References and Notes

(1) Hille, B. *Ionic channels of excitable membranes*; Sinauer Associates Inc.: Massachusetts, 1991.
(2) Voet, D.; Voet, J.G. *Biochemistry*, 3rd ed.; Wiley & Sons: New York, 2004; Vol. 1.
(3) MacKinnon, R. *Angew. Chem., Int. Ed.* **2004**, *43*, 4265.
(4) Ashcroft, F. M. *Nature* **2006**, *440*, 440.
(5) Ghadiri, M. R.; Granja, J. R.; Milligan, R. A.; McRee, D. E.; Khazanovich, N. *Nature* **1993**, *366*, 324.
(6) Ghadiri, M. R.; Granja, J. R.; Buehler, L. K. *Nature* **1994**, *369*, 301.
(7) Ghadiri, M. R.; Kobayashi, K.; Granja, J. R.; Chadha, R. K.; McRee, D. E. *Angew. Chem., Int. Ed. Engl.* **1995**, *34*, 93.
(8) Motesharei, K.; Ghadiri, M. R. *J. Am. Chem. Soc.* **1997**, *119*, 11306.
(9) Kim, H. S.; Hartgerink, J. D.; Ghadiri, M. R. *J. Am. Chem. Soc.* **1998**, *120*, 4417.
(10) Śanchez-Quesada, J.; Isler, M. P.; Ghadiri, M. R. *J. Am. Chem. Soc.* **2002**, *124*, 10004.
(11) Fernadez-Lopez, S.; Kim, H. S.; Choi, E. C.; Delgado, M.; Granja, J. R.; Khasanov, A.; Kraehenbuehl, K.; Long, G.; Weinberger, D. A.; Wilcoxen, K. M.; Ghadiri, M. R. *Nature* **2001**, *412*, 452.
(12) Engels, M.; Bashford, D.; Ghadiri, M. R. *J. Am. Chem. Soc.* **1995**, *117*, 9151.
(13) Asthagiri, D.; Bashford, D. *Biophys. J.* **2002**, *82*, 1176.
(14) Khurana, E.; Nielsen, S. O.; Ensing, B.; Klein, M. L. *J. Phys. Chem. B* **2006**, *110*, 18965−18972.
(15) Kurnikova, M. G.; Coalson, R. D.; Graf, P.; Nitzan, A. *Biophys. J.* **1999**, *76*, 642.
(16) van der Straaten, T. A.; Tang, J.; Eisenberg, R. S.; Ravaioli, U.; Aluru, N. R. *J. Comput. Electron.* **2002**, *1*, 335.
(17) Hwang, H.; Schatz, G. C.; Ratner, M. A. *J. Phys. Chem. B* **2006**, *110*, 6999.
(18) Bolhuis, P. G.; Dellago, C.; Chandler, D. *Proc. Natl. Acad. Sci.* **2000**, *97*, 5877.
(19) Allen, T. W.; Andersen, O. S.; Roux, B. *Proc. Natl. Acad. Sci. USA* **2004**, *101*, 117.
(20) Roux, B.; Allen, T.; Berneche, S.; Im, W. *Q. Rev. Biophys.* **2004**, *37*, 15.
(21) Liu, Z.; Xu, Y.; Tang, P. *J. Phys. Chem. B* **2006**, *110*, 12789.
(22) Pangali, C.; Rao, M.; Berne, B. J. *J. Chem. Phys.* **1979**, *71*, 2975.
(23) Kuharski, R. A.; Bader, J. S.; Chandler, D.; Sprik, M.; Klein, M. L.; Impey, R. W. *J. Chem. Phys.* **1988**, *89*, 3248.
(24) Roux, B. *Comput. Phys. Commun.* **1995**, *91*, 275.
(25) Hummer, G.; Szabo, A. *Proc. Natl. Acad. Sci. USA* **2001**, *98*, 3658.
(26) Jensen, M.O.; Park, S.; Tajkhorshid, E.; Schulten, K. *Proc. Natl. Acad. Sci. USA* **2002**, *99*, 6731.
(27) Park, S.; Khlili-Araghi, F.; Tajkhorshid, E.; Schulten, K. *J. Chem. Phys.* **2003**, *119*, 3559.
(28) Park, S.; Schulten, K. *J. Chem. Phys.* **2004**, *120*, 5946.
(29) Jarzynski, C. *Phys. Rev. Lett.* **1997**, *78*, 2690.
(30) Liphardt, J.; Dumont, S.; Smith, S. B.; Jr., I. T.; Bustamante, C. *Science* **2002**, *296*, 1832.
(31) *Spartan '04*; Wavefunction Inc.: Irvine, CA, 2004.
(32) MacKerell, A. D., Jr.; Bashford, D; Bellott, R. L. Dunbrack, R. L., Jr.; Evanseck, J. D.; Field, M. J.; Fischer, S.; Gao, J.; Guo, H.; Ha, S.; Joseph-McCarthy, D.; Kuchnir, L.; Kuczera, K.; Lau, F. T. K.; Mattos, C.; Michnick, S.; Ngo, T.; Nguyen, D. T.; Prodhom, B.; Reiher, W. E., III; Roux, B.; Schlenkrich, M.; Smith, J. C.; Stote, R.; Straub, J.; Watanabe, M.; Wiorkiewicz-Kuczera, J.; Yin, D.; Karplus, M. *J. Phys. Chem. B* **1998**, *102*, 3586.
(33) Kale, L.; Skeel, R.; Bhandarkar, M.; Brunner, R.; Gursoy, A.; Krawetz, N.; Phillips, J.; Shinozaki, A.; Varadarajan, K.; Schulten, K. *J. Comput. Chem.* **1999**, *151*, 283.
(34) Jorgensen, W. L.; Tirado-Rives, J. *J. Am. Chem. Soc.* **1988**, *110*, 1657.
(35) Beglov, D.; Roux, B. *J. Chem. Phys.* **1994**, *100*, 9050.
(36) Martínez, J. M.; Elmroth, S. K. C.; Kloo, L. *J. Am. Chem. Soc.* **2001**, *123*, 12279.
(37) Bogusz, S.; T. E. Cheatham, I.; Brooks, B. R. *J. Chem. Phys.* **1998**, *108*, 7070.
(38) Darden, T.; Pearlman, D.; Pedersen, L. G. *J. Chem. Phys.* **1998**, *109*, 10921.
(39) Humphrey, W.; Dalke, A.; Schulten, K. *J. Mol. Graphics* **1996**, *14*, 33.
(40) Balsera, M.; Stepaniants, S.; Izrailev, S.; Oono, Y.; Schulten, K. *Biophys. J.* **1997**, *73*, 1281.
(41) Jarzynski, C. *Phys. Rev. E* **1997**, *56*, 5018.
(42) Egolf, D. A. *Nature* **2002**, *296*, 1813.
(43) Parsegian, V. A. *Nature* **1969**, *221*, 844.
(44) Weetman, P.; Goldman, S.; Gray, C. G. *J. Phys. Chem. B* **1997**, *101*, 6073.
(45) Mamonov, A. B.; Coalson, R. D.; Nitzan, A.; Kurnikova, M. *Biophys. J.* **2003**, *84*, 3646.
(46) Beckstein, O.; Tai, K.; Sansom, M. S. P. *J. Am. Chem. Soc.* **2004**, *126*, 14694.
(47) Obst, S.; Bradaczek, H. *J. Chem. Phys.* **1996**, *100*, 15677.
(48) White, J. A.; Schwegler, E.; Galli, G.; Gygi, F. *J. Chem. Phys.* **2000**, *113*, 4668.
(49) Noskov, S. Y.; Berněche, S.; Roux, B. *Nature* **2004**, *431*, 830.
(50) Hyun, J.-K.; Babu, C. S.; Ichiye, T. *J. Phys. Chem.* **1995**, *99*, 5187.
(51) Lamm, G.; Pack, G. R. *J. Phys. Chem. B* **1997**, *101*, 959.
(52) Young, M. A.; Jayaram, B.; Beveridge, D. L. *J. Phys. Chem. B* **1998**, *102*, 7666.
(53) Chang, T.-M.; Dang, L. X. *J. Phys. Chem. B* **1999**, *103*, 4714.
(54) Shrivastava, I. H.; Tieleman, D. P.; Biggin, P. C.; Sansom, M. S. P. *Biophys. J.* **2002**, *83*, 633.
(55) Leung, K.; Rempe, S. B.; Lorenz, C. D. *Phys. Rev. Lett.* **2006**, *96*, 095504.